V European Conference on Computational Fluid Dynamics
ECCOMAS CFD 2010
J. C. F. Pereira and A. Sequeira (Eds)
Lisbon, Portugal, 14–17 June 2010

TIME DOMAIN BUFFETING ANALYSIS OF A LARGE-SPAN CABLE-STAYED BRIDGE

Shuxian Hong*, Álvaro Cunha*

*Faculty of Engineering of the University of Porto, Portugal
Rua Dr. Roberto Frias, 4200-465 Porto, Portugal
e-mail: edithhsx@gmail.com

Key words: Time Domain, Buffeting Analysis, Cable-stayed Bridge, Self-excited Forces

Abstract. *Large-span cable-stayed bridges are flexible structures susceptible to various types of wind-induced vibrations such as buffeting. In this study, a time domain buffeting analysis procedure is formulated and implemented by developing a toolbox based on ANSYS Parametric Design Language (APDL). To illustrate the potential of the toolbox, a real wind excited cable-stayed bridge built in China is taken as a case study. A comparison with results obtained including buffeting loads modeled by a quasi-steady approach is discussed. The results also show good agreement with those from the frequency domain analysis.*

1 INTRODUCTION

In the design and analysis of cable-stayed bridges, aerodynamic effects play an important role because of their high flexibility, low structural damping and light weight. Cable supported systems may be subjected to potentially large dynamic motions induced by wind forces. There are several mechanisms of interaction between wind and structure that produce structural vibrations; the mechanisms that are important to the bridge design are vortex shedding, galloping, flutter and buffeting. Unlike galloping, vortex shedding and flutter that can happen in a uniform flow without external disturbance, buffeting is a type of irregular vibration motion induced by turbulent wind in the bridge structure. The bridge response to buffeting depends on the turbulence intensity, shape of the structural elements and natural frequencies. Buffeting does not usually endanger the safety of the structure, but can result in discomfort for the users and lead to fatigue of structural elements.

In this study, a time domain buffeting analysis procedure is formulated and implemented by developing a toolbox based on ANSYS Parametric Design Language (APDL). To illustrate the potential of the toolbox, a real wind excited cable-stayed bridge built in China, the Qingzhou Bridge, is taken as a case study.

2 WIND FORCES FOR BUFFETING ANALYSIS

As it is assumed in classical airfoil theory, wind velocity at the points along the bridge has three components: the mean wind velocity U, the fluctuating part $u(x,t)$ in the along-wind direction and the fluctuating part $w(x,t)$ in the vertical direction. Due to the wind action, surface pressures arise on the contour of the section. The resultant of these pressures impose drag force D, lift force L and moment M.

Normally, the total wind load is made up of the steady state wind loads, the buffeting loads and the self-excited loads, and the governing equations are given in a matrix form by

$$M\ddot{\mathrm{X}} + C\dot{\mathrm{X}} + K\mathrm{X} = F_{se} + F_b + F_s \tag{1}$$

in which M, C and K are mass, damping and stiffness matrices respectively; X is the nodal displacement vector and F_b and F_{se} respect buffeting forces and self-excited forces respectively; F_s is the steady wind force, $F_s = \frac{1}{2}\rho U^2 B[C_D \quad C_L \quad BC_M]^T$, in which C_D, C_L and C_M are the coefficients of lift, drag and torsional moment of bridge deck, ρ is the air density; U is the mean wind speed and B is the deck width.

2.1 Buffeting forces

Buffeting forces are caused by the fluctuating component of the wind velocity. Buffeting forces of drag (D_b), lift (L_b), and torsional moment (M_b) per unit deck length are commonly expressed as follows [1]

$$D_b(t) = \frac{1}{2}\rho U^2 B\left(2C_D\chi_{Du}(K)\frac{u(t)}{U} + (C_D' - C_L)\chi_{Dw}(K)\frac{w(t)}{U}\right) \tag{2.a}$$

$$L_b(t) = \frac{1}{2}\rho U^2 B\left(2C_L\chi_{Lu}(K)\frac{u(t)}{U} + (C_L' + C_D)\chi_{Lw}(K)\frac{w(t)}{U}\right) \tag{2.b}$$

$$M_b(t)=\frac{1}{2}\rho U^2 B\left(2C_M\chi_{Mu}(K)\frac{u(t)}{U}+C'_M\chi_{Mw}(K)\frac{w(t)}{U}\right) \tag{2.c}$$

where u and w are the along-wind and vertical fluctuations of wind velocity respectively; C_D, C_L and C_M are the coefficients of lift, drag and torsional moment of bridge deck while C'_D, C'_L and C'_M are, respectively, the derivatives of C_D, C_L and C_M with respect to wind inclination; χ_{Du}, χ_{Dw}, χ_{Lu}, χ_{Lw}, χ_{Mu} and χ_{Mw} are the frequency-dependent aerodynamic admittance functions or transfer functions between velocity fluctuations and buffeting forces; $K = B\omega/U$ is the reduced frequency; and ω is the circular frequency of wind turbulence. In the case study presented in Section 4 all the aerodynamic admittance functions are assumed to be unit. This assumption may lead to overestimation of the bridge buffeting response.

2.2 Self-excited forces

The self-excited loads are caused by interaction between the wind motion and the structure. Self-excited loads are traditionally expressed in the form of indicial functions as suggested by Scanlan [2]. However, Lin [3] considered that there are some redundancies in the classical formulations. Based on the assumption that the self-excited loads are generated by linear mechanism, Lin suggested another simple mathematical model for self-excited forces for investigation of the aerodynamic stability of long-span suspension bridges. The self-excited loads are expressed in terms of convolution integrals between bridge deck motion and impulse response functions, which is shown to be equivalent to the classical indicial function type representation. Lin's model can be summarized as:

$$D_{se}(t)=D_\alpha(t)+D_h(t)=\int_{-\infty}^{t} f_{Dp}(t-\tau)p(t)d\tau+\int_{-\infty}^{t} f_{D\alpha}(t-\tau)\alpha(t)d\tau\,, \tag{3.a}$$

$$L_{se}(t)=L_\alpha(t)+L_h(t)=\int_{-\infty}^{t} f_{Lh}(t-\tau)h(t)d\tau+\int_{-\infty}^{t} f_{L\alpha}(t-\tau)\alpha(t)d\tau\,, \tag{3.b}$$

$$M_{se}(t)=M_\alpha(t)+M_h(t)=\int_{-\infty}^{t} f_{Mh}(t-\tau)h(t)d\tau+\int_{-\infty}^{t} f_{M\alpha}(t-\tau)\alpha(t)d\tau\,. \tag{3.c}$$

where $f_{Dp}(t)$, $f_{D\alpha}(t)$, $f_{L\alpha}(t)$, $f_{Lh}(t)$, $f_{M\alpha}(t)$ and $f_{Mh}(t)$ are response functions due to unit impulse displacement α, h and p. From these equations, it is seen that the aerodynamic coupling of the modes is induced by $D_\alpha(t)$, $L_\alpha(t)$ and $M_h(t)$.

Applying the Fourier transform to equations (3) and then comparing it with Scanlan's model in terms of aerodynamic derivatives, the relationship between transfer functions and aerodynamic derivatives can be obtained as:

$$F_{M\alpha}(\omega)=\rho B^4\omega^2\left[A_3^*+iA_2^*\right],\quad F_{Mh}(\omega)=\rho B^3\omega^2\left[A_4^*+iA_1^*\right], \tag{4.a,b}$$

$$F_{L\alpha}(\omega)=\rho B^3\omega^2\left[H_3^*+iH_2^*\right],\quad F_{Mh}(\omega)=\rho B^2\omega^2\left[H_4^*+iH_1^*\right], \tag{4.c,d}$$

$$F_{D\alpha}(\omega)=\rho B^3\omega^2\left[P_3^*+iP_2^*\right],\quad F_{Dh}(\omega)=\rho B^2\omega^2\left[P_4^*+iP_1^*\right] \tag{4.e,f}$$

where A^*_i and H^*_i (i=1,2,3,4) are non-dimensional flutter derivatives obtained by wind tunnel tests on a cross-section of the deck.

As for the introduction of the aerodynamic admittance functions, the definition of the self-excited forces on a deck section owes its origin to the studies made earlier on airfoils and thin-plates. Theodorsen [4], applying the potential flow theory, determined

analytically the self-excited forces acting on a thin airfoil undergoing crosswind and torsional complex sinusoidal motions. Following this approach, Scanlan and Tomko [5] defined the lift and the moment acting on a bridge deck section undergoing crosswind and torsional motions, as functions of suitably defined coefficients, called flutter derivatives. In the case of bridge deck sections, which have to be considered as bluff bodies, the flutter derivatives have to be determined experimentally by wind tunnel tests or by Computational Fluid Dynamics. Only six flutter derivatives (A_i^*, H_i^*, i=1,2,3) appeared in the original Scanlan and Tomko [5] formulation. With increasing spans, the importance of flutter derivatives associated with the motion in the alongwind direction was emphasized [6] and the complete set of the 18 flutter derivatives (A_i^*, H_i^*, P_i^*, i=1,…,6) is considered in recent works [7].

From classical air foil theory, the transfer functions may be reasonably approximated by rational functions, specifically for transfer functions of first order linear filters. The transfer functions can, therefore, be expressed as:

$$F_{Lh}(n)=\frac{1}{2}\rho\overline{U}^2\left(C_{1Lh}+i\frac{B}{\overline{U}}\frac{2\pi}{n}C_{2Lh}+\sum_{k=3}^{4}C_{kLh}\frac{i2\pi}{n\left(d_{kLh}\dfrac{\overline{U}}{B}+i\dfrac{2\pi}{n}\right)}\right), \tag{5.a}$$

$$F_{L\alpha}(n)=\frac{1}{2}\rho B\overline{U}^2\left(C_{1L\alpha}+i\frac{B}{\overline{U}}\frac{2\pi}{n}C_{2L\alpha}+\sum_{k=3}^{4}C_{kL\alpha}\frac{i2\pi}{n\left(d_{kL\alpha}\dfrac{\overline{U}}{B}+i\dfrac{2\pi}{n}\right)}\right), \tag{5.b}$$

$$F_{Mh}(n)=\frac{1}{2}\rho B\overline{U}^2\left(C_{1Mh}+i\frac{B}{\overline{U}}\frac{2\pi}{n}C_{2Mh}+\sum_{k=3}^{4}C_{kMh}\frac{i2\pi}{n\left(d_{kMh}\dfrac{\overline{U}}{B}+i\dfrac{2\pi}{n}\right)}\right), \tag{5.c}$$

$$F_{M\alpha}(n)=\frac{1}{2}\rho B^2\overline{U}^2\left(C_{1M\alpha}+i\frac{B}{\overline{U}}\frac{2\pi}{n}C_{2M\alpha}+\sum_{k=3}^{4}C_{kM\alpha}\frac{i2\pi}{n\left(d_{kM\alpha}\dfrac{\overline{U}}{B}+i\dfrac{2\pi}{n}\right)}\right). \tag{5.d}$$

Comparing equations (4) with equations (5), the flutter derivatives can be obtained as

$$H_1^*(K)=\frac{1}{K^2}\left(KC_{Lh2}+\sum_{k=3}^{4}\frac{C_{Lhk}d_{Lhk}(1/K)}{1+d_{Lhk}{}^2(1/K^2)}\right), \tag{6.a}$$

$$H_4(K)=\frac{1}{K^2}\left(C_{Lh1}+\sum_{k=3}^{4}\frac{C_{Lhk}}{1+d_{Lhk}{}^2(1/K^2)}\right), \tag{6.b}$$

$$H_2^*(K)=\frac{1}{K^2}\left(KC_{L\alpha 2}+\sum_{k=3}^{4}\frac{C_{L\alpha k}d_{L\alpha k}(1/K)}{1+d_{L\alpha k}{}^2(1/K^2)}\right), \tag{6.c}$$

$$H_3^*(K)=\frac{1}{K^2}\left(C_{L\alpha 1}+\sum_{k=3}^{4}\frac{C_{L\alpha k}}{1+d_{L\alpha k}{}^2\left(1/K^2\right)}\right), \tag{6.d}$$

$$A_1^*(K)=\frac{1}{K^2}\left(KC_{Mh2}+\sum_{k=3}^{4}\frac{C_{Mhk}d_{Mhk}\left(1/K\right)}{1+d_{Mhk}{}^2\left(1/K^2\right)}\right), \tag{6.e}$$

$$A_4^*(K)=\frac{1}{K^2}\left(C_{Mh1}+\sum_{k=3}^{4}\frac{C_{Mhk}}{1+d_{Mhk}{}^2\left(1/K^2\right)}\right), \tag{6.f}$$

$$A_2^*(K)=\frac{1}{K^2}\left(KC_{M\alpha 2}+\sum_{k=3}^{4}\frac{C_{M\alpha k}d_{M\alpha k}\left(1/K\right)}{1+d_{M\alpha k}{}^2\left(1/K^2\right)}\right), \tag{6.g}$$

$$A_3^*(K)=\frac{1}{K^2}\left(C_{M\alpha 1}+\sum_{k=3}^{4}\frac{C_{M\alpha k}}{1+d_{M\alpha k}{}^2\left(1/K^2\right)}\right). \tag{6.h}$$

In the above equations, K is the reduced frequency and is defined as $K=\frac{\omega B}{U}$. The unknown parameters C_{Lhk} , d_{Lhk} , $C_{L\alpha k}$, $d_{L\alpha k}$, C_{Mhk} , d_{Mhk} , $C_{M\alpha k}$ and $d_{M\alpha k}$, can be obtained from least-squares fitting of equations (6).

By taking the inverse Fourier transform of the transfer functions, the time domain expression of impulse response functions can be obtained. Substituting these impulse response functions into equation (5) yields

$$L_h(t)=\frac{1}{2}\rho B\overline{U}^2\left(C_{1Lh}\frac{h(t)}{B}+\frac{B}{\overline{U}}C_{2Lh}\frac{\dot{h}(t)}{B}+L_{h3}(t)+L_{h4}(t)\right), \tag{7.a}$$

$$L_\alpha(t)=\frac{1}{2}\rho B\overline{U}^2\left(C_{1L\alpha}\alpha(t)+\frac{B}{\overline{U}}C_{2L\alpha}\dot{\alpha}(t)+L_{\alpha 3}(t)+L_{\alpha 4}(t)\right), \tag{7.b}$$

$$M_h(t)=\frac{1}{2}\rho B^2\overline{U}^2\left(C_{1Mh}\frac{h(t)}{B}+\frac{B}{\overline{U}}C_{2Mh}\frac{\dot{h}(t)}{B}+M_{h3}(t)+M_{h4}(t)\right), \tag{7.c}$$

$$M_\alpha(t)=\frac{1}{2}\rho B^2\overline{U}^2\left(C_{1M\alpha}\alpha(t)+\frac{B}{\overline{U}}C_{2M\alpha}\dot{\alpha}(t)+M_{\alpha 3}(t)+M_{\alpha 4}(t)\right) \tag{7.d}$$

in which, for k=3, 4:

$$L_{hk}(t)=C_{Lhk}\int_{-\infty}^{t}\frac{\dot{h}(\tau)}{B}e^{-\frac{d_{Lhk}\overline{U}}{B}(t-\tau)}d\tau\ , \tag{8.a}$$

$$L_{\alpha k}(t)=C_{L\alpha k}\int_{-\infty}^{t}\dot{\alpha}(\tau)e^{-\frac{d_{L\alpha k}\overline{U}}{B}(t-\tau)}d\tau, \tag{8.b}$$

$$M_{hk}(t)=C_{Mhk}\int_{-\infty}^{t}\frac{\dot{h}(\tau)}{B}e^{-\frac{d_{Mhk}\overline{U}}{B}(t-\tau)}d\tau, \tag{8.c}$$

$$M_{\alpha k}(t)=C_{M\alpha k}\int_{-\infty}^{t}\dot{\alpha}(\tau)e^{-\frac{d_{M\alpha k}\overline{U}}{B}(t-\tau)}d\tau, \tag{8.d}$$

Regarding the motion history parts, it can be seen that the items involve convolution integrals of velocities. These series integrals can be summarized as:

$$I_j = \int_{-\infty}^{t_j} \exp\left[(-d_i U / B)(t_j - \tau)\right]\dot{\delta}(\tau)d\tau \tag{9}$$

It can be seen that for calculating their values, the integral I_j must be evaluated at every time step t_j, which is quite time consuming. Besides, the motion history for all elements must be stored, thus occupying a large computer memory. To tackle these difficulties, a recursive algorithm for evaluating the integral is derived as follows [8]:

$$I_j = \exp\left[(-d_i U / B)(t_j - t_{j-1})\right]I_{j-1} + \exp\left[(-d_i U / B)(t_j - t_{j-1})\right]\Delta\delta_{j-1} \tag{10}$$

From the above equation, it can be seen that only the quantities involving I_{j-1} and δ_{j-1} at time t_{j-1} need to be stored for evaluating I_j.

Equation (7) can thus be further written in the matrix form as the function of the modal coordinates of the bridge.

$$F_{se} = C_{ae}\dot{\mathrm{X}} + K_{ae}\mathrm{X} + \hat{F}_{se} \tag{11}$$

The elements of matrices $C_{se}, K_{se}, \hat{F}_{se}$ in Equation (11) can be respectively given by:

$$K_{ae} = \frac{1}{2}\rho U^2 B\begin{bmatrix} 0 & 0 & 0 \\ 0 & C_{1Lh} & BC_{1L\alpha} \\ 0 & BC_{1Mh} & B^2C_{1M\alpha} \end{bmatrix}, \tag{12.a}$$

$$C_{ae} = \frac{1}{2}\rho U^2 B/U\begin{bmatrix} 0 & 0 & 0 \\ 0 & C_{2Lh} & BC_{2L\alpha} \\ 0 & BC_{2Mh} & B^2C_{2M\alpha} \end{bmatrix}, \tag{12.b}$$

$$\hat{F}_{se} = \begin{Bmatrix} 0 \\ L_{h3}(t)+L_{h4}(t)+L_{\alpha 3}(t)+L_{\alpha 4}(t) \\ M_{h3}(t)+M_{h4}(t)+M_{\alpha 3}(t)+M_{\alpha 4}(t) \end{Bmatrix}. \tag{12.c}$$

3 DYNAMIC MODEL FOR BUFFETING ANALYSIS

The equations of motion for a bridge in turbulent flow can be expressed as:

$$M\ddot{\mathrm{X}} + \overline{C}\dot{\mathrm{X}} + \overline{K}\mathrm{X} = \hat{F}_{se} + F_b + F_s \tag{13}$$

where

$$\overline{C} = C - C_{ae},\ \overline{K} = K - K_{ae}$$

The effect of aeroelastic stiffness and damping can be model by *Matrix27* in ANSYS. *Matrix27* represents an arbitrary element whose geometry is undefined but whose elastic kinematic response can be specified by stiffness, damping or mass coefficients in matrix form. The matrix is assumed to relate two nodes, each with six degrees of freedom per node. Note that one *Matrix27* element can only model C_{ae} or K_{ae}. To simulate both the aeroelastic stiffness and damping effect of bridge in buffeting analysis, an integrated finite element model can be developed which consists of a particular structural element *e* and two fictitious *Matrix27* elements. As shown in Fig. 1, a pair of Matrix27 elements is attached to each element *e* of the bridge to simulate the aeroelastic forces acting on two nodes. The two *Matrix27* elements are separately plotted in the

figure for clarity. Element *e1* is employed to model aerodynamic stiffness and element *e2* is used to model aerodynamic damping. Elements *e*, *e1* and *e2* share the same nodes, *i* and *j*. The elemental aeroelastic stiffness matrix K_{ae}^{e} and aeroelastic damping matrix C_{ae}^{e} for the element *e*, respectively, and their expressions in the form of consistent formulation are given in the Appendix.

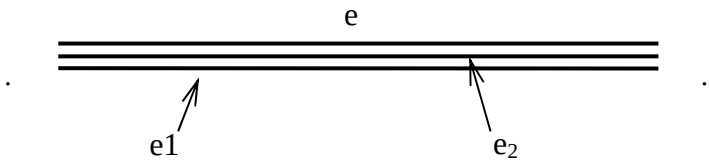

Fig. 1 Finite element model formulated in *ANSYS* to account for self-excited forces

4 CASE STUDY

4.1 Bridge description and main parameters

In this section the time domain procedure is used to analyse the buffeting response of Qingzhou Bridge. This is a cable-stayed bridge (Fig. 2) with a composite-deck system consisting of five spans with an overall length of 1186.34m (41.13m + 250m + 605m + 250m + 40.21m). The two diamond-shaped towers are of reinforced concrete. The height of the towers is 175.5m with 145.5m above the bridge deck. The clear navigation is 43m.

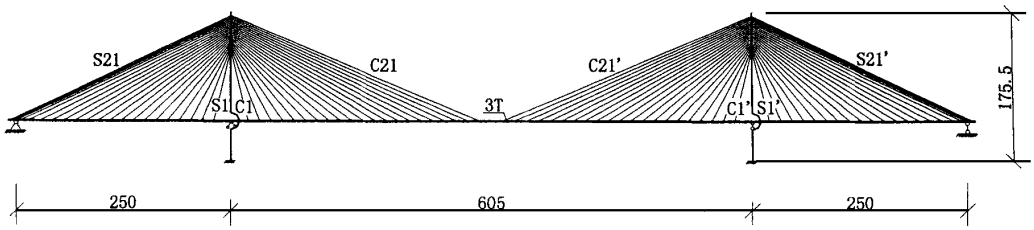

Fig. 2 Elevation of Qingzhou Bridge (Unit: m).

The composite-deck system (Fig. 3) of the bridge has an open-section consisting of two main I-type steel girders, steel floor beams and 25cm thickness concrete slab. The slender steel girder is 2.45m high and its maximum plate thickness reaches 80mm. The ratio of girder height to span length is about 1/202. One steel stringer is designed in the middle of the cross-section. There are in total 257 steel floor beams with a spacing of 4.5m. The precast concrete slab is connected to the steel girders and floor beams by shear studs.

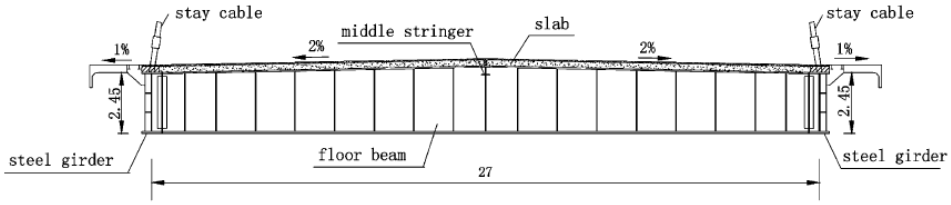

Fig. 3 Typical cross-section of composite deck of Qingzhou Bridge . (Unit: m)

A three-dimensional finite-element model of the bridge was established and the natural frequencies and mode shapes were computed. The calculated natural frequencies and mode shapes were verified through comparison with the measured results, and the details can be found in ref. [9] and [10].

The steady aerodynamic parameters of the section at 0° wind attack angle are $C_D = 1.365$, $C'_D = 1.116$, $C_M = 0.042$, $C'_M = 1.116$, $C_l = -0.179$, $C'_l = 4.14$. Six flutter derivatives (Appendix 2) obtained from wind tunnel test (at *State Key Laboratory for Disaster Reduction in Civil Engineering, Tongji University, Shanghai, China*) are shown in Fig. 4, as well as the fitting curves respectively.

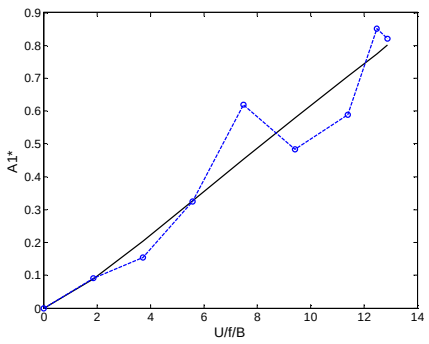

a. Flutter derivative A_1^* and corresponding fitting curve

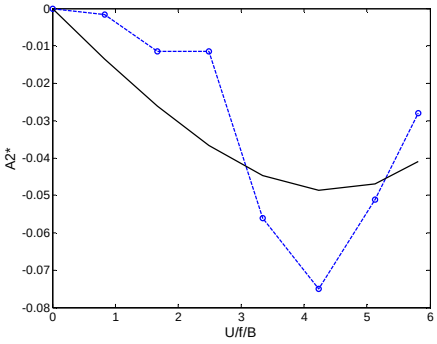

b. Flutter derivative A_2^* and corresponding fitting curve

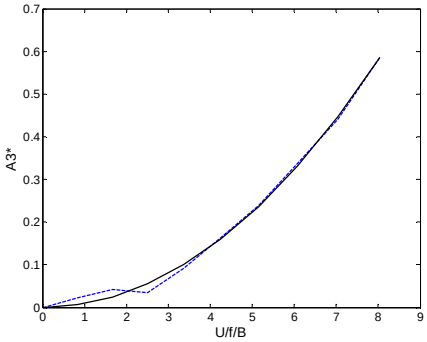

c. Flutter derivative A_3^* and corresponding fitting curve

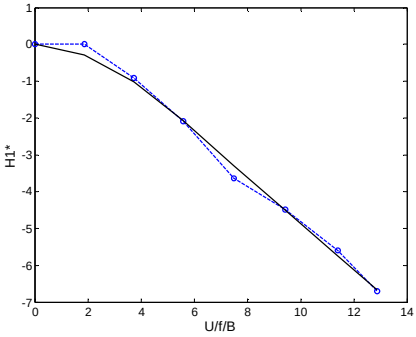

d. Flutter derivative H_1^* and corresponding fitting curve

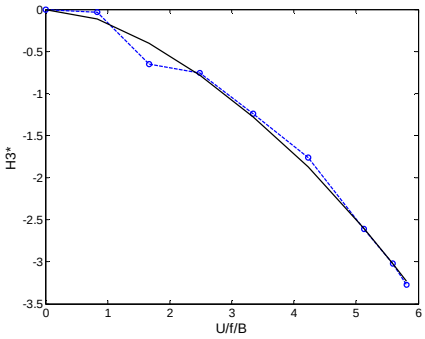

e. Flutter derivative H_2^* and corresponding fitting curve

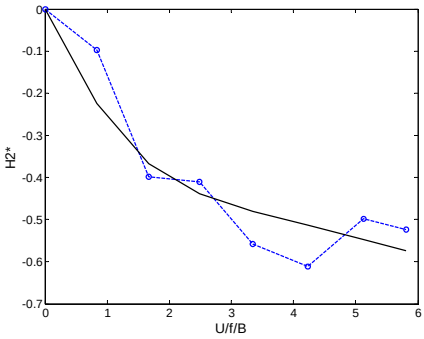

f. Flutter derivative H_3^* and corresponding fitting curve

Fig. 4 Six flutter derivatives obtained from wind tunnel tests

The relationships between A_2^*, A_4^*, H_2^* and H_4^* are given by [11,12]:

$$A_4^* = -kA_2^*, \quad H_4^* = -kH_2^* \tag{14}$$

From least-squares fitting of equations (6), the indicial function coefficients C_{Lhk}, d_{Lhk}, $C_{L\alpha k}$, $d_{L\alpha k}$, C_{Mhk}, d_{Mhk}, $C_{M\alpha k}$ and $d_{M\alpha k}$, can be obtained. Due to the lack of wind tunnel test results on lateral flutter derivatives P_i^*, only the vertical and rotational motions of the bridge deck are taken into account in the simulation of self-excited forces.

4.2 Simulation of wind velocity

The wind velocity field on the bridge deck is assumed to be composed of 87 wind velocity waves at 87 different points distributed along the deck of the bridge. According to the Chinese code, the following longitudinal and vertical wind power spectra are adopted:

a) Along wind direction - Davenport spectrum:

$$S_v(n) = U_{10}^2 \frac{4kx^2}{n(1+x^2)^{4/3}} \tag{15}$$

where n is the frequency of turbulence wind, k is the roughness factor of ground, U_{10} is the mean velocity at a height of 10m and $x = 1200\dfrac{n}{U_{10}^2}$.

b) Vertical direction - Panofsky spectrum:

$$S_w(z,n) = U_*{}^2 \frac{3.36 \cdot \dfrac{n \cdot z}{\overline{U}(z)}}{n\left(1+10\dfrac{n \cdot z}{\overline{U}(z)}\right)^{5/3}} \tag{16}$$

where $U_* = \dfrac{kv}{\lg\left(\dfrac{z-z_d}{z_0}\right)}$, $z_d = H_0 - z_0/k$ and H_0 is the mean height of building around the bridge.

The mean wind speed at the deck level is taken as 46.3m/s, and the sampling frequency and duration used in the simulation of wind speed are, respectively, 10 Hz and 409.6s. Fig. 5 shows the simulated time-histories of horizontal and vertical fluctuating wind speeds, respectively, at the middle of the main-span of the bridge.

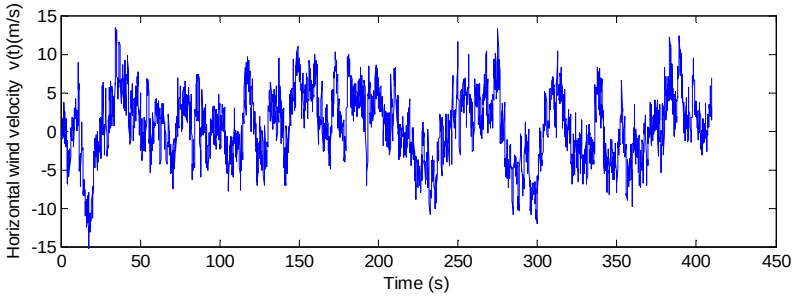

(a)

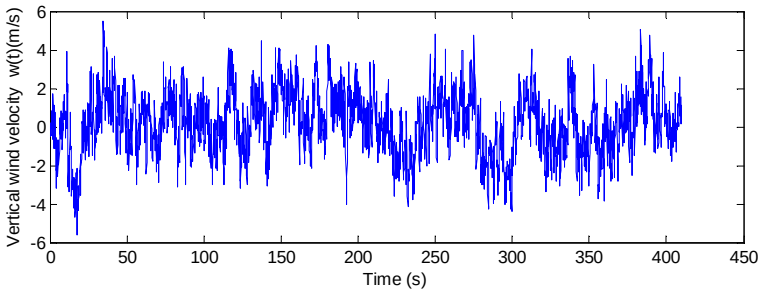

(b)

Fig.5 Simulated wind velocities at middle of the main-span: (a) horizontal fluctuating wind velocity $u(t)$; (b) vertical fluctuating wind velocity $w(t)$

4.3 Buffeting responses of the Qingzhou Bridge

Displayed in Figures 6(a-c) are the response time-history of the vertical, lateral and torsional displacement. Figures 7(a,b) plot the spectra of vertical and lateral displacements at the mid-span. The identified dominant frequencies are in accordance with the 1st vertical and 1st transversal bending modes, respectively.

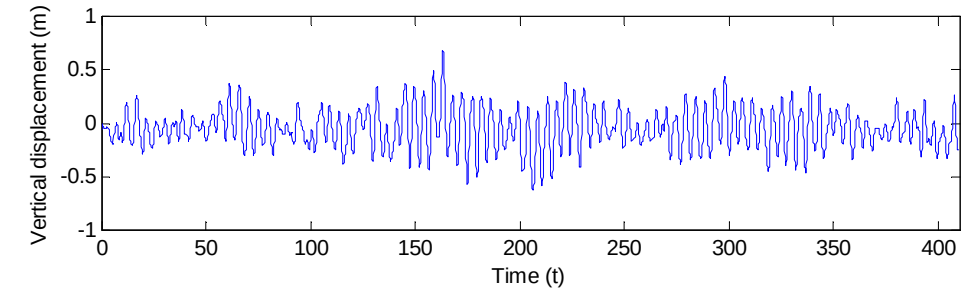

(a)

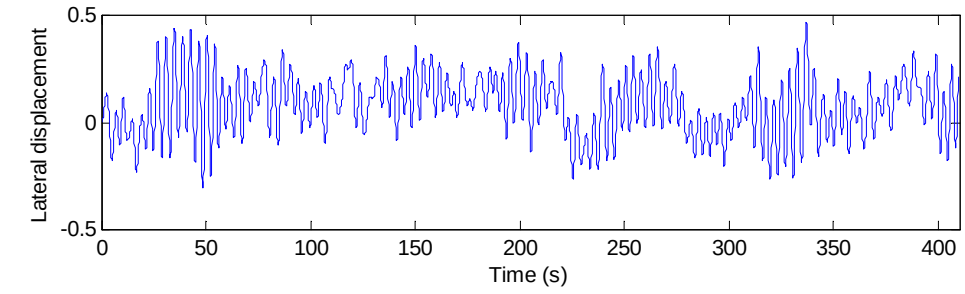

(b)

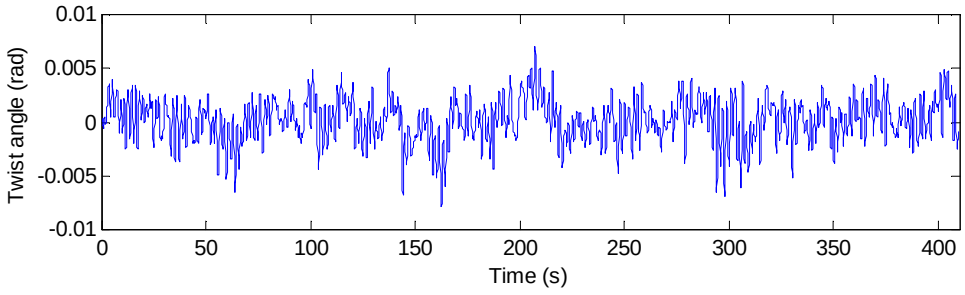

(c)

Fig. 6 Dynamic displacement responses of bridge at mid span: (a) vertical displacement response; (b) lateral displacement response; (c) torsional displacement response

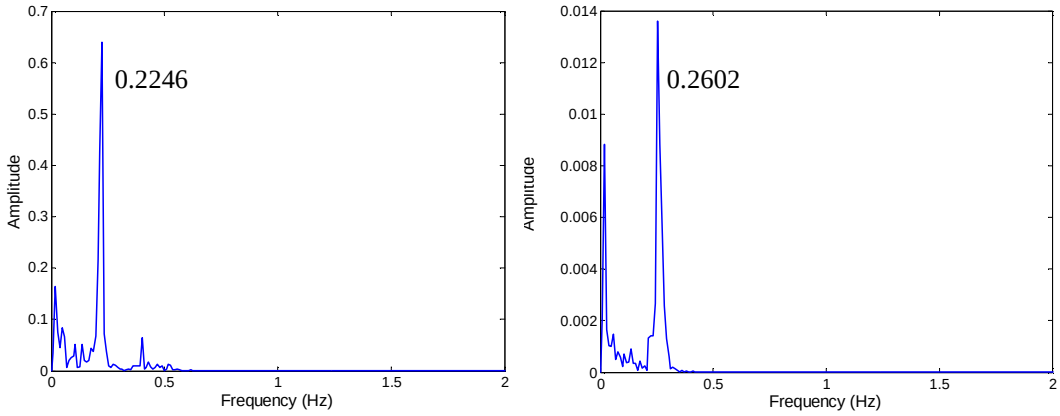

(a) (b)

Fig. 7 Spectra of vertical (a) and lateral displacements (b) at mid-span

Figures 8(a,b) show the distributions of the maximum vertical deflections and the lateral displacements of the bridge deck along its span. It is seen that the fluctuating wind components have stronger influence on the lateral displacement than on the vertical deflection.

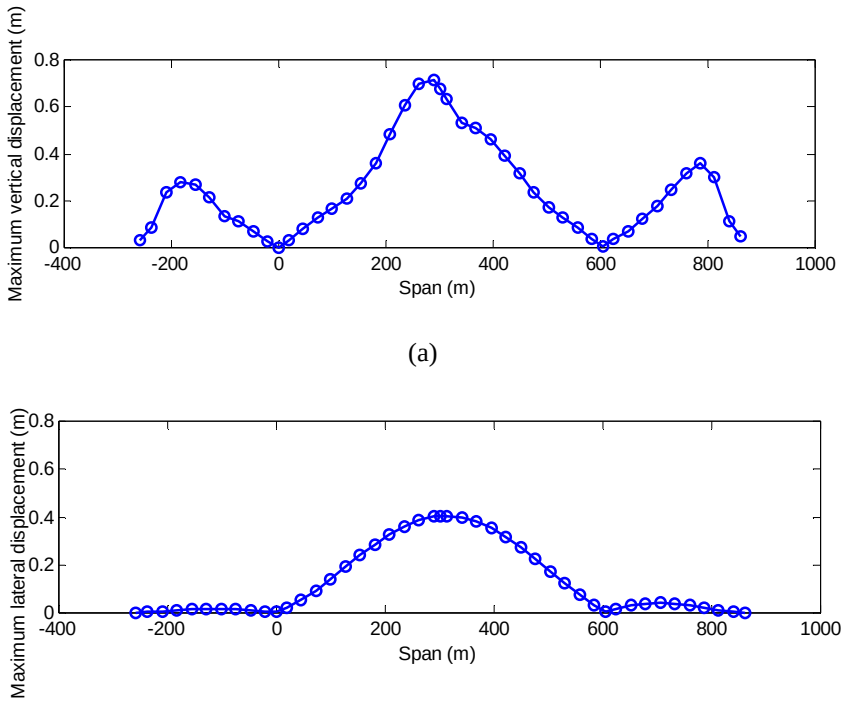

(a)

(b)

Fig. 8 Maximum vertical (a) and lateral (b) displacements along the span

The results (Case 3) can be now compared with the ones from other two cases: Case 1 - without considering self-excited forces; Case 2 - self-excited forces evaluated by quasi-steady theory [13]. Fig. 9 shows the RMS of vertical displacement responses at mid span obtained in Case 1 and Case 2 comparing with the result without considering self-excited forces, at mean wind velocities $U = 34, 38, 42, 46 m/s$. It is shown that the results obtained considering self-excited forces are smaller than those obtained without considering self-excited forces. The reason is that the aeroelastic damping has often a

mitigating effect caused by positive aerodynamic damping at lower wind velocities. The results obtained in case 3 are about 7% smaller than in case 2.

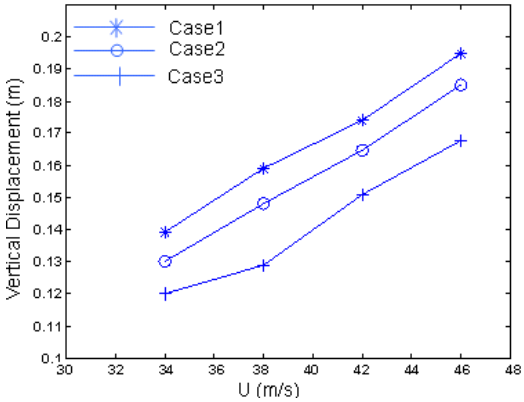

Fig. 9 Variation of RMS of vertical displacement at mid span

Ref. [14] presents a frequency domain buffeting analysis in the context of the design of Qingzhou Bridge. The vertical buffeting response at mid span is given as 0.23m.

5 CONCLUSIONS

A framework has been presented in this paper to investigate the buffeting response of large-span bridges. Computer simulation techniques were used to generate wind forces and self-excited forces, based on measured aerodynamic coefficients and flutter derivatives. A toolbox was developed based on ANSYS Parametric Design Language (APDL) and used to perform a case study. The results showed that the formulation presented in this paper could predict the buffeting response of large-span bridges, and led to results inferior to the ones obtained by quasi-steady approach. The comparison with the results of frequency domain analysis shows also reasonable agreement.

REFERENCES

[1] R.H SCANLAN, Aeroelastic simulation of bridges, 1983, Journal of Structural Engineering, ASCE 109, 2829-2837.

[2] R. H. SCANLAN, J. G. BELIVEAU and K. S. BUDLONG, Indicial aerodynamic functions for bridge decks. Journal of Engineering Mechanics, ASCE 100 (1974), pp. 657–672.

[3] C. G. BUCHER and Y. K. LIN, Stochastic stability of bridges considering coupled modes. Journal of Engineering Mechanics, ASCE 114 (1988), pp. 2055–2071.

[4] T. Theodorsen, General theory of aerodynamic instability and the mechanism of flutter, NACA Report 496, US Nat. Advisory Committee for Aeronautics, Langley, VA 1935.

[5] R.H. Scanlan, J.J. Tomko, Airfoil and bridge deck flutter derivatives, J. Eng. Mech. Div. ASCE 97 (EM6) (1971) 1717–1737.

[6] R.H. Scanlan, On flutter and buffeting mechanisms in long-span bridges, Prob. Eng. Mech. 3 (1) (1988) 22–27.

[7] Alexandre de la Foye，Calcul de la reponse dynamique des structures elancees a la turbulence du vent，Thèse de doctorat，le 9 juillet 2001，Universite de Nantes ecole Doctorale

[8] Q. Ding, P. K. K. Lee and S. H. Lo, Time domain buffeting analysis of suspension bridges subjected to turbulent wind with effective attack angle, Journal of sound and vibration (2000) 233(2),311-327

[9] Wei-Xin Ren, Xue-Lin Peng, 2005, Computer & Structures 83, 536-550. Baseline finite element modeling of a large span cable-stayed bridge through field ambient vibration tests.

[10] Wei-Xin Ren, You-Qin Lin and Xue-Lin Peng, 2007, J. Bridge Engineering ASCE, Volume 12, Issue 2, pp. 261-270, Field Load Tests and Numerical Analysis of Qingzhou Cable-Stayed Bridge.

[11] R.H. Scanlan, N.P. Jones and L. Singh, Inter-relations among flutter derivatives, J. Wind Eng. Ind. Aerodyn. 69–71 (1997), pp. 829–837.

[12] F.Tubino, Relationships among aerodynamic admittance functions, flutter derivatives and static coefficients for long span bridges. Journal of Wind Engineering and Industrial Aerodynamics, Volume 93, Issue 21, December, pp. 929-950

[13] Z.Q. Chen, Y. Han, X.G. Hu, Y.Z. Luo, Investigation On Influence Factors Of Buffeting Response Of Bridges And Its Aeroelastic Model Verification For Xiaoguan Bridge. Journal of Engineering Structures, 31(2009), pp. 417-431.

[14] Ha Hong, Buffeting analysis and calculation of internal force of Qingzhou Cable-stayed bridge caused by wind. Journal of Tongji University. Volum 29, No.1, Jan. 2001

APPENDIX

$$K_{ae}^{e} =$$

$$\frac{1}{2}\rho U^2 L \begin{bmatrix}
0 & 0 & 0 & 0 & 0 & 0 & 0 & 0 & 0 & 0 & 0 & 0 \\
0 & 0 & 0 & 0 & 0 & 0 & 0 & 0 & 0 & 0 & 0 & 0 \\
0 & 0 & \frac{13}{35}h_k & \frac{7}{20}k_k & \frac{11L}{210}h_k & 0 & 0 & 0 & \frac{9}{70}h_k & \frac{3}{20}k_k & \frac{-13L}{420}h_k & 0 \\
0 & 0 & \frac{7B}{20}i_k & \frac{B}{3}m_k & \frac{BL}{20}i_k & 0 & 0 & 0 & \frac{3B}{20}i_k & \frac{B}{6}m_k & \frac{-LB}{30}i_k & 0 \\
0 & 0 & \frac{11L}{210}h_k & \frac{L}{20}k_k & \frac{L^2}{105}h_k & 0 & 0 & 0 & \frac{13L}{420}h_k & \frac{L}{30}k_k & \frac{-L^2}{140}h_k & 0 \\
0 & 0 & 0 & 0 & 0 & 0 & 0 & 0 & 0 & 0 & 0 & 0 \\
0 & 0 & 0 & 0 & 0 & 0 & 0 & 0 & 0 & 0 & 0 & 0 \\
0 & 0 & 0 & 0 & 0 & 0 & 0 & 0 & 0 & 0 & 0 & 0 \\
0 & 0 & \frac{9}{70}h_k & \frac{3}{20}k_k & \frac{13L}{420}e_k & 0 & 0 & 0 & \frac{13}{35}h_k & \frac{7}{20}k_k & \frac{-11L}{210}h_k & 0 \\
0 & 0 & \frac{3B}{20}i_k & \frac{B}{6}m_k & \frac{BL}{30}i_k & 0 & 0 & 0 & \frac{7B}{20}i_k & \frac{B}{3}m_k & \frac{-BL}{20}i_k & 0 \\
0 & 0 & \frac{-13L}{420}h_k & \frac{-L}{30}k_k & \frac{-L^2}{140}e_k & 0 & 0 & 0 & \frac{-11L}{210}h_k & \frac{-L}{20}k_k & \frac{L^2}{105}h_k & 0 \\
0 & 0 & 0 & 0 & 0 & 0 & 0 & 0 & 0 & 0 & 0 & 0
\end{bmatrix}$$

in which

$h_k = L \cdot C_{Lh1}$; $k_k = L \cdot C_{L\alpha 1} \cdot B$; $i_k = L \cdot C_{Mh1}$; $m_k = L \cdot C_{M\alpha 1} \cdot B$; $e_k = L \cdot C_{Lh1}$.

$$C_{ae}^{e} =$$

$$\frac{1}{2}\rho U^2 BL/U \begin{bmatrix}
0 & 0 & 0 & 0 & 0 & 0 & 0 & 0 & 0 & 0 & 0 & 0 \\
0 & 0 & 0 & 0 & 0 & 0 & 0 & 0 & 0 & 0 & 0 & 0 \\
0 & 0 & \frac{13}{35}h_c & \frac{7}{20}k_c & \frac{11L}{210}h_c & 0 & 0 & 0 & \frac{9}{70}h_c & \frac{3}{20}k_c & \frac{-13L}{420}h_c & 0 \\
0 & 0 & \frac{7B}{20}i_c & \frac{B}{3}m_c & \frac{BL}{20}i_c & 0 & 0 & 0 & \frac{3B}{20}i_c & \frac{B}{6}m_c & \frac{-LB}{30}i_c & 0 \\
0 & 0 & \frac{11L}{210}h_c & \frac{L}{20}k_c & \frac{L^2}{105}h_c & 0 & 0 & 0 & \frac{13L}{420}h_c & \frac{L}{30}k_c & \frac{-L^2}{140}h_c & 0 \\
0 & 0 & 0 & 0 & 0 & 0 & 0 & 0 & 0 & 0 & 0 & 0 \\
0 & 0 & 0 & 0 & 0 & 0 & 0 & 0 & 0 & 0 & 0 & 0 \\
0 & 0 & 0 & 0 & 0 & 0 & 0 & 0 & 0 & 0 & 0 & 0 \\
0 & 0 & \frac{9}{70}h_c & \frac{3}{20}k_c & \frac{13L}{420}e_c & 0 & 0 & 0 & \frac{13}{35}h_c & \frac{7}{20}k_c & \frac{-11L}{210}h_c & 0 \\
0 & 0 & \frac{3B}{20}i_c & \frac{B}{6}m_c & \frac{BL}{30}i_c & 0 & 0 & 0 & \frac{7B}{20}i_c & \frac{B}{3}m_c & \frac{-BL}{20}i_c & 0 \\
0 & 0 & \frac{-13L}{420}h_c & \frac{-L}{30}k_c & \frac{-L^2}{140}e_c & 0 & 0 & 0 & \frac{-11L}{210}h_c & \frac{-L}{20}k_c & \frac{L^2}{105}h_c & 0 \\
0 & 0 & 0 & 0 & 0 & 0 & 0 & 0 & 0 & 0 & 0 & 0
\end{bmatrix}$$

in which

$h_c = L \cdot C_{Lh2}$; $k_c = L \cdot C_{L\alpha 2} \cdot B$; $i_c = L \cdot C_{Mh2}$; $m_c = L \cdot C_{M\alpha 2} \cdot B$; $e_c = L \cdot C_{Lh2}$.